









## Diurnal and Seasonal Variations of Aerosol Optical Depth Observed by MEDA/TIRS at Jezero Crater, Mars



### Special Section:

The Mars Perseverance Rover  
Jezero Crater Floor Campaign

Michael D. Smith<sup>1</sup> , Germán M. Martínez<sup>2</sup> , Eduardo Sebastián<sup>3</sup>, Mark T. Lemmon<sup>4</sup> ,  
Michael J. Wolff<sup>4</sup> , Victor Apéstigue<sup>3</sup> , Ignacio Arruego<sup>3</sup> , Daniel Toledo<sup>3</sup> ,  
Daniel Viúdez-Moreiras<sup>3</sup> , Jose Antonio Rodriguez-Manfredi<sup>3</sup>, and Manuel de la Torre Juarez<sup>5</sup>

### Key Points:

- The Thermal InfraRed Sensor (TIRS) upward-looking sensors enable the retrieval of total aerosol optical depth during both day and night
- Aerosol optical depth shows clear diurnal and seasonal trends. Diurnal maximum opacity is near dawn for clouds and near noon for dust
- TIRS retrievals of aerosol optical depth can detail the complex time history of rapidly changing events such as dust storms

<sup>1</sup>NASA Goddard Space Flight Center, Greenbelt, MD, USA, <sup>2</sup>Lunar and Planetary Institute/USRA, Houston, TX, USA, <sup>3</sup>Centro de Astrobiología (INTA-CSIC), Madrid, Spain, <sup>4</sup>Space Science Institute, Boulder, CO, USA, <sup>5</sup>Jet Propulsion Laboratory, California Institute of Technology, Pasadena, CA, USA

### Correspondence to:

M. D. Smith,  
[Michael.D.Smith@nasa.gov](mailto:Michael.D.Smith@nasa.gov)

### Citation:

Smith, M. D., Martínez, G. M., Sebastián, E., Lemmon, M. T., Wolff, M. J., Apéstigue, V., et al. (2023). Diurnal and seasonal variations of aerosol optical depth observed by MEDA/TIRS at Jezero Crater, Mars. *Journal of Geophysical Research: Planets*, 128, e2022JE007560. <https://doi.org/10.1029/2022JE007560>

Received 2 SEP 2022  
Accepted 21 DEC 2022

**Abstract** The two upward-looking Thermal InfraRed Sensor (TIRS) channels from the Mars Environmental Dynamics Analyzer (MEDA) instrument suite on board the Perseverance rover enable the retrieval of total aerosol optical depth (dust plus water ice cloud) above the rover for all observations when TIRS is taken. Because TIRS observes at thermal infrared wavelengths, the retrievals are possible during both the day and night and thus, they provide an excellent way to monitor both the diurnal and seasonal variations of aerosols above Jezero Crater. A retrieval algorithm has been developed for this purpose and here, we describe that algorithm along with our results for the first 400 sols of the Perseverance mission covering nearly the entire aphelion season as well as a regional dust storm and the beginning of the perihelion season. We find systematic diurnal variations in aerosol optical depth that can be associated with dust and water ice clouds as well as a clear change from a cloud-filled aphelion season to a perihelion season where dust is the dominant aerosol. A comparison of retrieved optical depths between TIRS and the SkyCam camera that is also part of MEDA indicates evidence of possible diurnal variations in cloud height or particle size.

**Plain Language Summary** Observations made by the Thermal InfraRed Sensor (TIRS) instrument on the Perseverance rover enable the amount of airborne dust and clouds above the rover to be determined. The TIRS instrument observes thermal infrared radiation so it can observe the dust and clouds both during the day and night. Here, we present results for the first 13 months of observations by TIRS. These results show that the dust and clouds vary as a function of season on Mars and as a function of the time of day. At the beginning of the period of time studied here, there were more clouds than dust, and the clouds were maximum just before dawn and just after dusk. Later in the season, dust became the dominant aerosol, with the diurnal maximum near midday.

## 1. Introduction

Dust and water ice aerosols greatly influence the current climate of Mars through their role in modifying the solar and infrared radiation fields throughout the atmosphere (e.g., Clancy et al., 2017; Gierasch & Goody, 1972; Kahre et al., 2017; Wolff et al., 2017). Therefore, the characterization of these aerosols and their dynamics remains a key goal of Mars atmospheric science and is an important part of creating accurate numerical models, especially on the relatively short timescales associated with dynamic events such as dust lifting, dust devils, cloud formation, and the development of dust storms (e.g., Kahre et al., 2006; Newman et al., 2002; Newman et al., 2021; Pla-Garcia et al., 2020; Rafkin et al., 2016; Wu et al., 2021).

The Perseverance rover landed on the surface of Mars at Jezero Crater (18.4°N, 77.5°W) on 18 February 2021 (Mars Year 36,  $L_s = 6^\circ$ ). Contained in the collection of scientific instruments on board the rover is the Mars Environmental Dynamics Analyzer (MEDA), which is a suite of different sensors placed throughout the rover with the goal of characterizing and studying the near-surface meteorology at the rover location (J. A. Rodriguez-Manfredi et al., 2021). A set of MEDA sensors, collectively called the Thermal Infrared Sensor (TIRS), has the goal of measuring the upward and downward radiation fields and energy budget at the surface (Martínez et al., 2023; Pérez-Izquierdo et al., 2018; Sebastián et al., 2020, 2021).

The observations by the two upward-looking TIRS sensors enable the retrieval of total aerosol optical depth in the column of atmosphere above the rover. While this type of observation of aerosol optical depth has previously been

© 2023 Jet Propulsion Laboratory, California Institute of Technology and The Authors. Government sponsorship acknowledged. This article has been contributed to by U.S. Government employees and their work is in the public domain in the USA.  
This is an open access article under the terms of the [Creative Commons Attribution-NonCommercial-NoDerivs License](https://creativecommons.org/licenses/by-nc-nd/4.0/), which permits use and distribution in any medium, provided the original work is properly cited, the use is non-commercial and no modifications or adaptations are made.

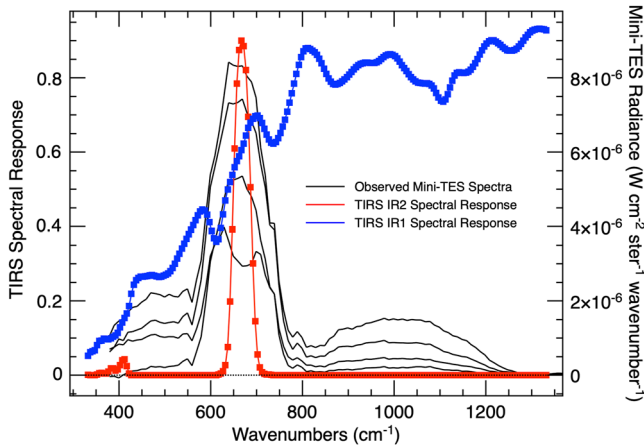


**Figure 1.** The spectral response of the Thermal InfraRed Sensor (TIRS) IR1 (blue) and IR2 (red) sensors compared with typical observed Miniature Thermal Emission Spectrometer (Mini-TES) spectra (black). The different Mini-TES spectra represent different atmospheric temperatures and different amounts of aerosol loading showing the sensitivity of TIRS IR1 and IR2 to those quantities.

performed many times from previous landers and rovers (e.g., Chen-Chen et al., 2019; Colburn et al., 1989; Lemmon et al., 2004, 2015; M. D. Smith et al., 2016; P. H. Smith & Lemmon, 1999) and can be performed using other instruments on the Perseverance rover, what makes the TIRS observations special is the fact that they are taken at thermal infrared wavelengths and can therefore provide retrievals of aerosols during the night as well as during the day. Indeed, the thermal-infrared spectra obtained by the Miniature Thermal Emission Spectrometer (Mini-TES) spectrometers on board the Mars Exploration Rovers demonstrated this ability, but Mini-TES observations during the night were severely limited in number by power constraints (Mason & Smith, 2021; M. D. Smith et al., 2004, 2006).

In this paper, we present results of the retrieval of total aerosol optical depth from the upward-looking TIRS sensors taken during the first 13 months of Perseverance operations. In Section 2 we describe the TIRS data set and the algorithm we have developed to perform the retrieval. In Section 3, we present a summary of the retrieval results, providing an overview of the seasonal and diurnal variations of aerosol optical depth observed so far. Section 4 describes additional analysis of the results, including an attempt to separate the contributions of dust and water ice aerosol and a comparison of our TIRS retrievals against the concurrent observations of aerosol optical depth by the SkyCam. Finally, we provide a summary of our work in Section 5.

## 2. Data Set and Retrieval Algorithm

### 2.1. TIRS Instrument and Data

TIRS is a set of five radiometers designed to characterize the upward and downward thermal infrared radiation at the surface, the reflected shortwave solar radiation from the surface, the surface temperature, and atmospheric temperature near the surface (Sebastián et al., 2020, 2021). TIRS is one part of the MEDA suite of sensors on the Perseverance rover (J. A. Rodriguez-Manfredi et al., 2021). Of interest here are the sensors: TIRS IR1, which covers a broad portion of the thermal-infrared spectrum over the range 6–35  $\mu\text{m}$  and TIRS IR2, which covers a portion of the  $\text{CO}_2$  band between 14.5 and 15.5  $\mu\text{m}$  as shown in Figure 1. Both sensors view upward at an elevation angle centered 35° above the rover deck. The field of view of the TIRS IR1 and IR2 sensors is 20° in the vertical direction and 40° in the horizontal direction.

As part of the MEDA suite of atmospheric sensors, TIRS observations are typically taken systematically throughout each sol at a frequency of 1 Hz. During the period of time considered here, observations in 1-hr blocks were generally taken so that odd-numbered hours were covered on odd-numbered sols, while even-numbered hours were covered on even-numbered sols. In that way, the entire 24-hr diurnal cycle could be fully covered over a span of two sols. Occasionally, additional one-hour blocks were added to this baseline providing additional coverage and observations were also routinely taken during the first 5 minutes of every hour. These observations were a part of the background baseline set for MEDA observations that ran almost every sol providing excellent diurnal and seasonal coverage.

Figure 1 shows the spectral response of the TIRS channels IR1 and IR2 along with the observed spectra from the Mini-TES (Christensen et al., 2003). In the Mini-TES spectra, the band of strong emission between 550 and 750  $\text{cm}^{-1}$  is caused by  $\text{CO}_2$  gas and was used to retrieve atmospheric temperatures in the lowest 2 km of the atmosphere (M. D. Smith et al., 2006). The broad emissions outside of that (350–550 and 750–1,300  $\text{cm}^{-1}$ ) are caused by dust and water ice aerosol. The TIRS IR1 channel essentially includes the entire thermal-infrared spectral range, including contributions from both  $\text{CO}_2$  and aerosols, while the TIRS IR2 channel covers only the central portion of the  $\text{CO}_2$  gas band. The calibrated data files produced by TIRS (the “CAL” datafiles available from the Planetary Data System) give IR1 measurements in terms of an integrated flux ( $\text{W m}^{-2}$ ), while the IR2 measurements are given in terms of an effective temperature, which can be integrated using its spectral response to produce a flux measurement if desired.

In general, the observed signals from TIRS IR1 and IR2 are sensitive to a combination of the atmospheric opacity (from aerosols and gases) and the atmospheric temperature profile. In practice, because of the very high opacity

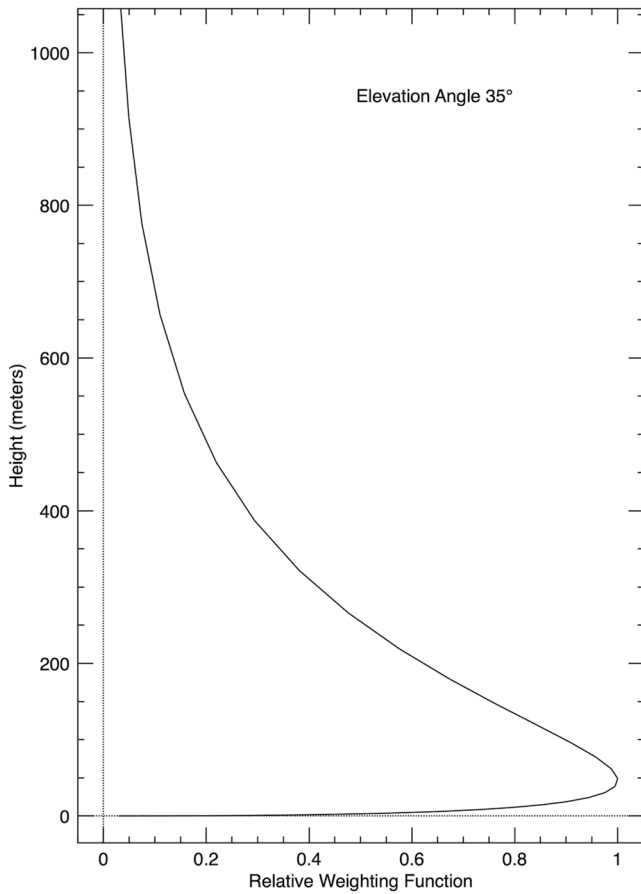


**Figure 2.** The weighting function for the Thermal InfraRed Sensor IR2 sensor at the nominal elevation angle of  $35^\circ$  above the horizon. Although the peak of the weighting function peaks at an altitude of  $\sim 40$  m, there is a significant contribution from atmospheric layers from just above the surface to several hundred meters above the surface.

of  $\text{CO}_2$  in the middle of the  $15\text{-}\mu\text{m}$  band compared to aerosols, the signal in that spectral range is only sensitive to atmospheric temperatures in the lowest few km of the atmosphere and is nearly insensitive to aerosols. For example, in Figure 1 within the spectral range dominated by  $\text{CO}_2$  between  $550$  and  $750\text{ cm}^{-1}$  ( $13.3\text{--}18.2\text{ }\mu\text{m}$ ), the differences in radiance between the four Mini-TES spectra are caused by differences in atmospheric temperatures in the lowest 2 km of the atmosphere (e.g., M. D. Smith et al., 2006), with the lowest spectra showing a nighttime case with lower atmospheric temperatures. On the other hand, outside the  $\text{CO}_2$  band at longer wavelengths ( $350\text{--}550$ ) and at shorter wavelengths ( $750\text{--}1,300\text{ cm}^{-1}$ ), the radiance is sensitive to both atmospheric temperatures and aerosol optical depth.

Figure 2 shows the weighting function (e.g., Petty, 2006) for the TIRS IR2 sensor at a nominal elevation angle of  $35^\circ$  above the horizon and typical atmospheric temperatures. The curve would shift upward or downward slightly for elevation angles higher or lower, respectively, than  $35^\circ$ . The peak of this weighting function lies at roughly 40 m and the observed IR2 temperature is often referred to as being representative of temperatures at that level. However, in reality, the temperature observed by IR2 is representative of a broad layer of the atmosphere from just above the surface to several hundred meters above the surface.

## 2.2. Aerosol Optical Depth Retrieval Algorithm

We use a radiative transfer model to compute the expected TIRS IR1 and IR2 signals for a given aerosol optical depth and temperature profile. We can then perform the retrieval by varying the atmospheric temperatures and aerosol optical depth until the computed IR1 and IR2 match the values observed by TIRS. The radiative transfer model is based on that used for the Mini-TES retrievals (M. D. Smith et al., 2004, 2006). Given the upward-viewing geometry, including aerosol scattering is essential and is included in this model using a 2-stream approximation. The absorption by  $\text{CO}_2$  gas is treated using the correlated-k approximation (Lacis & Oinas, 1991). The elevation angle above the horizon for the TIRS field of view is important and is computed for each observation using the known pitch, roll, and yaw of the Perseverance rover. Surface temperature is taken directly from the TIRS IR5 sensor observations.

As a baseline in our model, we use the temperature profile returned from the Mars Climate Database (MCD) (Forget et al., 1999; Millour et al., 2018) for the given latitude, longitude, local time (LT), and  $L_s$  of each observation. We then modified this profile using the observed TIRS IR2 temperature. We use our radiative transfer model to compute the expected IR2 signal and we offset the MCD temperature profile in the lowest 1 km until the computed IR2 signal matches the observed signal. The top panel of Figure 3 shows the magnitude of this shift in atmospheric temperature. The offsets are typically no larger than a few K.

The temperature profile above an altitude of 10 km is estimated using concurrent observations taken by the EMIRS thermal-infrared spectrometer on board the Emirates Mars Mission (Edwards et al., 2021; M. D. Smith et al., 2022). This difference is shown in the bottom panel of Figure 3 and is also typically a few K outside of the period after  $L_s = 150^\circ$ , when there was a large regional dust storm (Lemmon et al., 2022; M. D. Smith et al., 2022, see Section 3.3 below). The temperature profile from the MCD is then used to help link the two regions between where EMIRS and TIRS IR2 are sensitive.

Once the temperature profile has been estimated, we are left with a single observation (TIRS IR1) and a single unknown (total aerosol optical depth), which results in the straightforward task of varying aerosol optical depth in our radiative transfer model until the computed IR1 value matches the observed value. This one-parameter fit does not require any complicated minimization techniques and can be performed using standard root-finding algorithms.

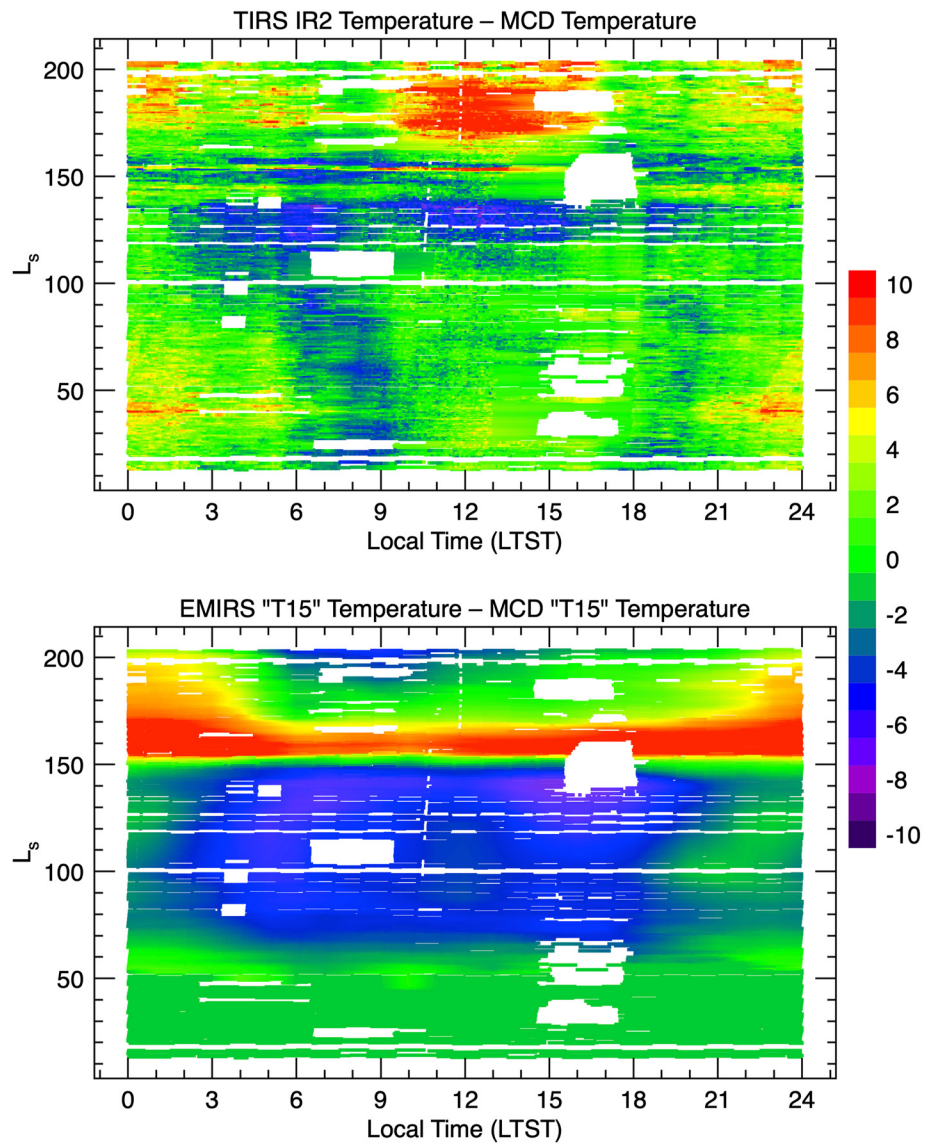


**Figure 3.** (Top panel) The temperature differences between observed Thermal InfraRed Sensor (TIRS) IR2 and the equivalent temperature (i.e., lowest 1 km above the surface) from the Mars Climate Database (MCD). (Bottom panel) The temperature difference between the EMIRS “T15” temperature (i.e., temperature at ~25 km altitude) and that given by the MCD. These corrections are applied to the MCD temperature profile before performing the retrieval for aerosol optical depth using TIRS IR1.

Given that we have only one observation (TIRS IR1) for the retrieval of aerosol optical depth, the relative contributions from dust and water ice cloud cannot in general be uniquely separated using the TIRS data alone. Therefore, to perform the retrieval, we assume a seasonally dependent dust versus ice fraction based on the climatology derived from previous observations (e.g., M. D. Smith, 2004) and the concurrent retrievals from EMIRS (M. D. Smith et al., 2022). Specifically, for all local times, we assume a 1:2 ratio for dust versus ice during the first portion of the period (until  $L_s = 151^\circ$ ) and then a 4:1 ratio after that. In practice, although the absolute values of the total aerosol optical depth depend somewhat on this apportionment, the overall seasonal and diurnal patterns in the retrieved total aerosol optical depth are not very sensitive to this fraction for any reasonable values.

Aerosol physical properties were taken from the analysis of Mini-TES data by Wolff et al. (2006). An effective radius of  $1.5 \mu\text{m}$  is assumed for dust and  $2.0 \mu\text{m}$  for water ice cloud to be consistent with previous work. The vertical distribution of the dust is taken to follow a Conrath profile (Conrath, 1975) with the Conrath- $\nu$  parameter

chosen so that the top of the dust is at 2 scale heights above the surface. Water ice clouds are placed at one scale height above the surface with a scale height of one half of the pressure scale height (i.e., about 5 km).

### 2.3. Uncertainties

The uncertainties in the observed TIRS IR1 flux as reported in the TIRS datafiles are roughly 5%–10% during the night and 15%–20% during the day. At the relatively low optical depths typically observed at Mars, this would correspond directly to uncertainties in the retrieved optical depth with the same percentages. A closer examination of the TIRS data shows that estimate to be conservative, and likely representative more of accuracy than precision. The reported uncertainty of TIRS IR2 is 1–2 K, which would translate to an uncertainty in the retrieved optical depth of  $\sim 0.01$ – $0.02$ .

Beyond the uncertainties related directly to the data themselves are systematic uncertainties related to the assumptions and approximations made in the retrieval algorithm and radiative transfer model. These include such things as use of the 2-stream approximation for aerosol scattering instead of a higher order approximation, the apportionment of dust and water ice aerosol, the vertical distributions of the aerosol, the particle size of the aerosols, and the atmospheric temperatures. All of these can be evaluated through numerical experiments, and their effects range from negligible (e.g., use of the 2-stream approximation) to potentially large (e.g., vertical distribution of aerosols). However, if we discount unlikely scenarios (e.g., errors in the temperature profile of 20+ K, or all the dust being confined to the lowest 1 km), we find that these systematic uncertainties do not dominate the accuracy estimates mentioned above.

In summary, we estimate a total uncertainty in the aerosol optical depth values retrieved here to be at the upper end of the accuracy uncertainty, or 10% during the night and 20% during the day. The “noise” level in the retrievals represented by the retrieval-to-retrieval variance in consecutive retrievals is substantially less, implying that the precision of the retrievals is likely better than the uncertainty values quoted above. Larger systematic errors in retrieved values caused by inaccurate assumptions are possible but would tend to shift all retrieved values in the same direction, leaving the diurnal patterns described here mostly unchanged.

## 3. Aerosol Optical Depth Results

Figure 4 shows the retrieved aerosol optical depth for TIRS observations taken during the 13 months between sol 15 (5 March 2021, MY 36,  $L_s = 13^\circ$ ) and sol 400 (4 April 2022, MY 36,  $L_s = 204^\circ$ ) as a function of season ( $L_s$ ) and local true solar time (LTST). Retrievals are performed on 5-min blocks of data, which are the averages of 300 individual TIRS observations. Shown here is the total aerosol extinction optical depth, which includes scattering. This optical depth is the sum of the contribution from dust, which is referenced to  $1,075 \text{ cm}^{-1}$  ( $9 \mu\text{m}$ ), plus the contribution from water ice cloud, which is referenced to  $825 \text{ cm}^{-1}$  ( $12 \mu\text{m}$ ).

The generally excellent coverage of MEDA observations is evident in Figure 4. The gaps that appear during the mid-morning and especially the mid-afternoon are periods of time when the Sun was within the TIRS field-of-view. Those data have been excluded since those results are often unreliable. Shorter gaps (generally overnight) are times when the TIRS instrument ran calibration sequences that precluded normal observations.

### 3.1. Overall Climatology

An overview of all the retrievals of aerosol optical depth from TIRS observations is presented in Figure 4. The retrievals began near the start of the aphelion season with relatively low aerosol optical depth. The optical depth gradually increased as the aphelion season progressed, and during this season there was a clear and consistent diurnal variation of aerosol optical depth with highest values between 05:00 and 09:00 and a minimum at around 16:00. All local times quoted in this work are LTST. This diurnal variation is almost certainly caused by a variation in water ice clouds, which is superimposed on top of a baseline of dust optical depth. While there is a clear seasonal trend, there is also a significant variation from one sol to the next, which is most likely caused by water ice clouds as well.

The aerosol optical depth decreased after  $L_s = 120^\circ$  only to increase again at  $L_s = 140^\circ$  for a week or two ( $\sim 5^\circ$  of  $L_s$ ). After a brief clearing, there was a very significant increase in optical depth indicated by the red band in Figure 4 at  $L_s = 153^\circ$ , which was an early-season regional dust storm (e.g., Lemmon et al., 2022; M. D. Smith

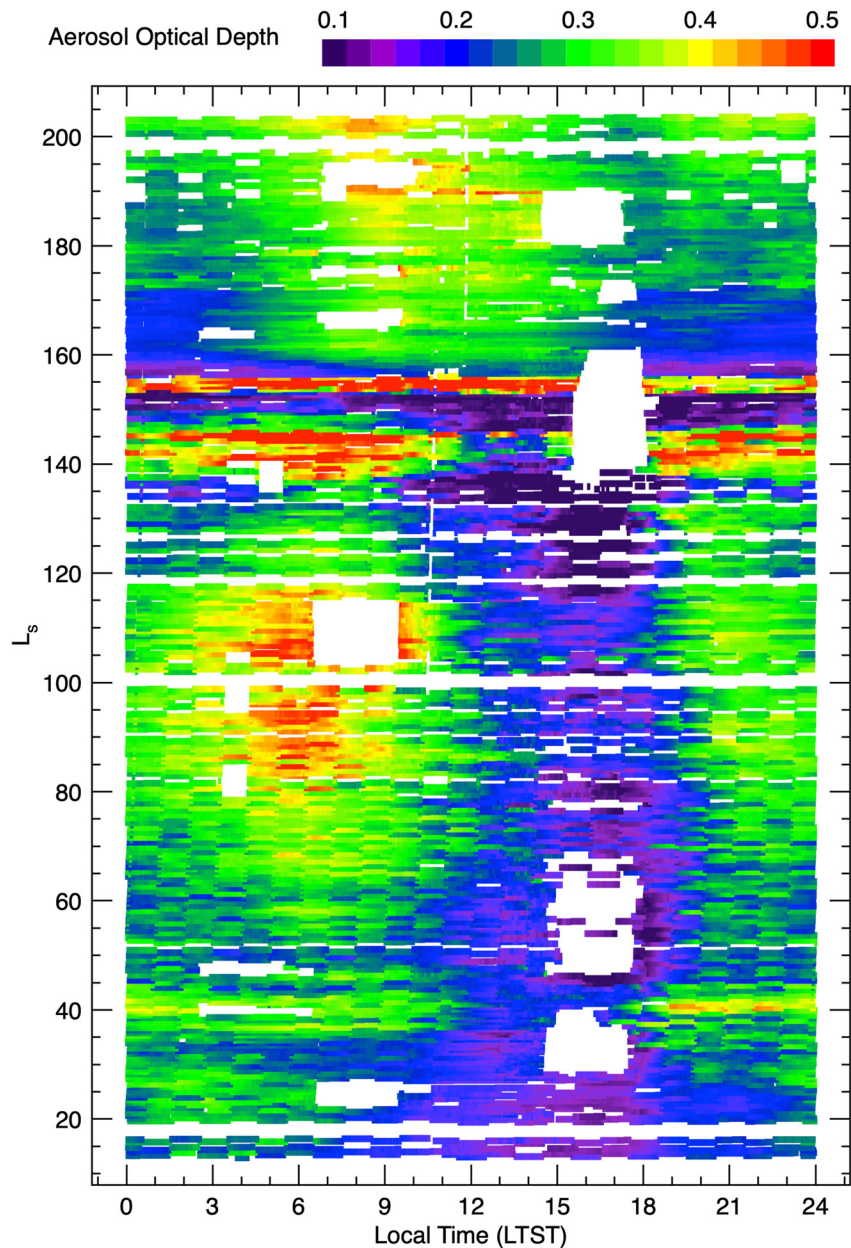


**Figure 4.** An overview of all the Thermal InfraRed Sensor retrieval results showing the diurnal (local true solar time) and seasonal ( $L_s$ ) variation of total aerosol optical depth. Included during this period were the aphelion season cloud belt ( $L_s \sim 30^\circ\text{--}150^\circ$ ), a regional dust storm ( $L_s = 153^\circ\text{--}156^\circ$ ), and the transition to the perihelion season after  $L_s = 180^\circ$ .

et al., 2022). After the dust storm cleared, there was a general and gradual increase in opacity heading into the perihelion season, where it is expected that dust would become the dominant aerosol over water ice clouds. These observations taken after the regional dust storm showed a higher overall baseline of aerosol optical depth (likely caused by dust) but with some water ice clouds still present. The LT variation was distinctly different than during the aphelion season with the diurnal maximum moving later toward the middle of the day.

### 3.2. Aphelion-Season Cloud Belt

The lower two-thirds of Figure 4 from approximately  $L_s = 30^\circ$  until  $L_s = 150^\circ$  is the season of the aphelion cloud belt, which has been observed numerous times before (e.g., Clancy et al., 2017; M. D. Smith, 2004 and references therein). The optical depth of the clouds grew steadily after  $L_s = 50^\circ$  reaching its peak at roughly  $L_s = 100^\circ$  before a more rapid decrease in clouds after  $L_s = 120^\circ$ . Interestingly, at both the beginning and

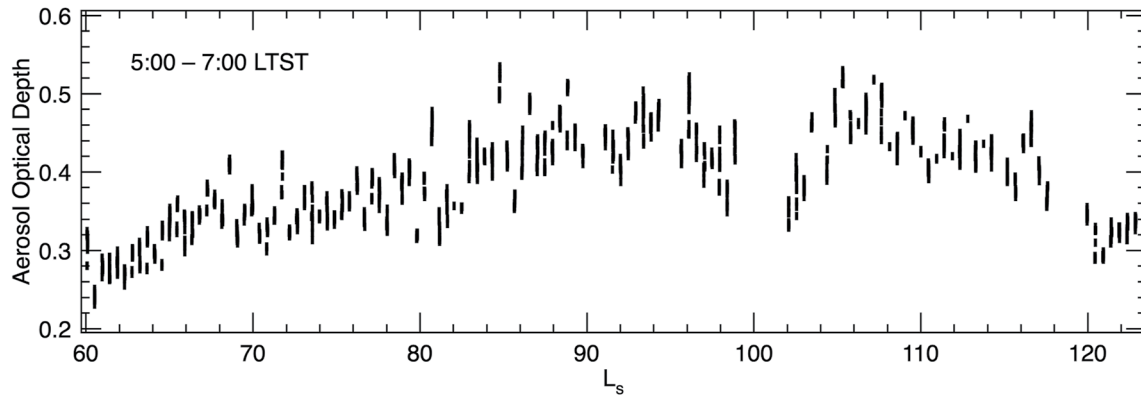


**Figure 5.** The retrieved aerosol optical depth between 05:00 and 07:00 local true solar time during the middle of the aphelion season. Each bar represents the range of aerosol optical depth between 05:00 and 07:00 for each sol of observations. There was a significant sol-to-sol variation in the observed optical depth.

ending of the aphelion cloud season there were local maxima in the cloud optical depth at both  $L_s = 40^\circ$  and  $140^\circ$ , symmetric about the northern winter solstice. The later peak at  $L_s = 140^\circ$  was particularly strong with aerosol optical depth exceeding the maximum values of the main peak of cloud activity around  $L_s = 100^\circ$ . Throughout the aphelion cloud season, the diurnal variation of aerosol optical depth was remarkably consistent, with a primary maximum near 06:00, a secondary maximum near 22:00, and minimum daily optical depth near 16:00.

Figure 5 shows the retrieved total aerosol optical depth during the daily maximum between 05:00 and 07:00 during the middle of the aphelion season. Each bar in the figure represents all the observations during this LT interval for one sol. The differences in optical depth from one sol to the next are often greater than the range of variation within a sol implying that there were significant sol-to-sol variations in the amount of clouds over the rover site. This sol-to-sol variability is most apparent in Figure 4 during the early morning hours when cloud opacity is greatest, but it is also present during the evening.

### 3.3. Regional Dust Storm

Figure 6 shows the complex time history of aerosol optical depth during the January 2022 regional dust storm event. Observations by other instruments on the Perseverance rover (Lemmon et al., 2022) and by other spacecraft (M. D. Smith et al., 2022) have conclusively identified this activity as a large early-season regional dust storm that initiated north and east of Hellas before rapidly overrunning the Perseverance site on sol 313 (5 January 2022,  $L_s = 153^\circ$ ). Over the next several sols, the TIRS retrievals show both a significant increase in the baseline aerosol (dust) optical depth as well as numerous discrete spikes in the optical depth. These spikes had optical depths exceeding 0.7 (at  $9 \mu\text{m}$ ) and lasted from one to several hours. They occurred preferentially during daytime hours, although equally in the morning and afternoon.

By sol 319 (11 January 2022,  $L_s = 156^\circ$ ), the active portion of the storm had significantly subsided at the Perseverance site leaving behind an increased aerosol loading with a different diurnal variation than existed before the dust storm (see also Figure 4). In particular, the maximum diurnal aerosol optical depth shifted several hours later, from 06:00 before the dust storm to near noon after the storm. Presumably, this shift reflects the change in the dominant aerosol from water ice cloud to dust as observed by other spacecraft (M. D. Smith et al., 2022, see also the discussion in Section 4.1).

## 4. Discussion

### 4.1. Dust Versus Water Ice Clouds

Although we cannot retrieve independent values for dust and water ice cloud aerosol optical depth from the TIRS observations alone, it is apparent from looking at Figure 4 that there are at least two distinct components that contribute to the total optical depth that is retrieved. We envisage that the total optical depth,  $\tau(\text{sol}, \text{LT})$ , is a function of sol and LT, and can be expressed as the sum of two components:

$$\tau(\text{sol}, \text{LT}) = S_1(\text{sol}) D_1(\text{LT}) + S_2(\text{sol}) D_2(\text{LT}) \quad (1)$$

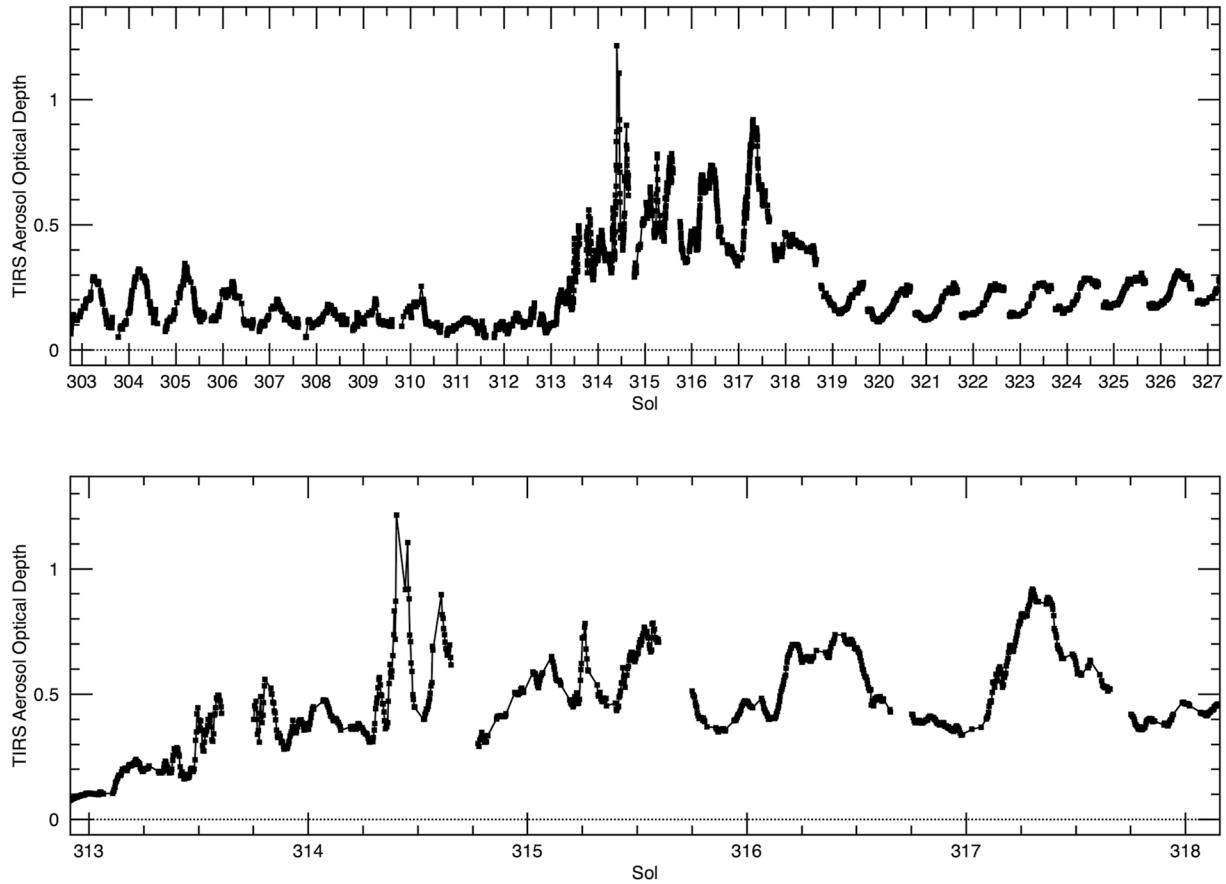


**Figure 6.** Retrieved total aerosol optical depth from Thermal InfraRed Sensor as a function of time (sol) showing the regional dust storm of January 2022. Here, the sol numbers label midnight local true solar time. (Top panel) The 4-week period between late December 2021 and mid-January 2022, or  $L_s = 148^\circ$ – $161^\circ$ . (Bottom panel) The same data focusing on the 5 sols (313–317) covering the most active period of the storm (5–9 January 2022,  $L_s = 153^\circ$ – $156^\circ$ ).

Here, the two “S” functions describe the amplitude of each component as a function of sol (or  $L_s$ ), while the two “D” functions describe the amplitude of each component as a function of LT. We further assume that the diurnal variations,  $D_i(LT)$ , can be expressed in the form of a sum of harmonics:

$$D_i(LT) = 1 + \alpha_{1,i} \cos[\phi - \phi_{1,i}] + \alpha_{2,i} \cos[2(\phi - \phi_{2,i})] + \alpha_{3,i} \cos[3(\phi - \phi_{3,i})] + \dots \quad (2)$$

The parameter  $\phi$  describes LT in terms of an angle (i.e.,  $\phi = 15 \times LT$ , if expressed in degrees), and the constant “1” as the first term in the expansion ensures that the diurnally averaged value of  $D_i(LT)$  is unity.

We implemented a least squares fitting of the above by expressing the sol dependence,  $S(\text{sol})$ , every 10 sols ( $5^\circ$  of  $L_s$ ) for a total of 39 free parameters for each of the two components, and by keeping the first three harmonics (after the constant) of the diurnal variation for six more free parameters per component. Given the large number of parameters (90) to fit, we attempted the least squares fitting using a number of different starting conditions, including all free parameters being zero. In the fitting, we excluded the period of the regional dust storm (sols 311–319) since we did not expect the optical depth to follow the form of Equation 1 during an active dust storm. The solution was found to be robust, always arriving at essentially the same two components. Experiments with additional terms in the harmonic expansion of the diurnal variation (Equation 2) showed negligible improvement in the fit after the third harmonic.

The diurnal variation ( $D_1$  and  $D_2$ ) and seasonal variation ( $S_1$  and  $S_2$ ) of those two components are shown in Figure 7. The seasonal variation of the two components shows that until  $L_s = 150^\circ$  component 2 had greater amplitude than component 1, while after that (i.e., after the regional dust storm) component 1 dominated over component 2. Based on climatology (e.g., M. D. Smith, 2004) and concurrent observations by orbiters (e.g., M. D. Smith et al., 2022), this seasonal dependence strongly suggests that component 1 is associated with dust



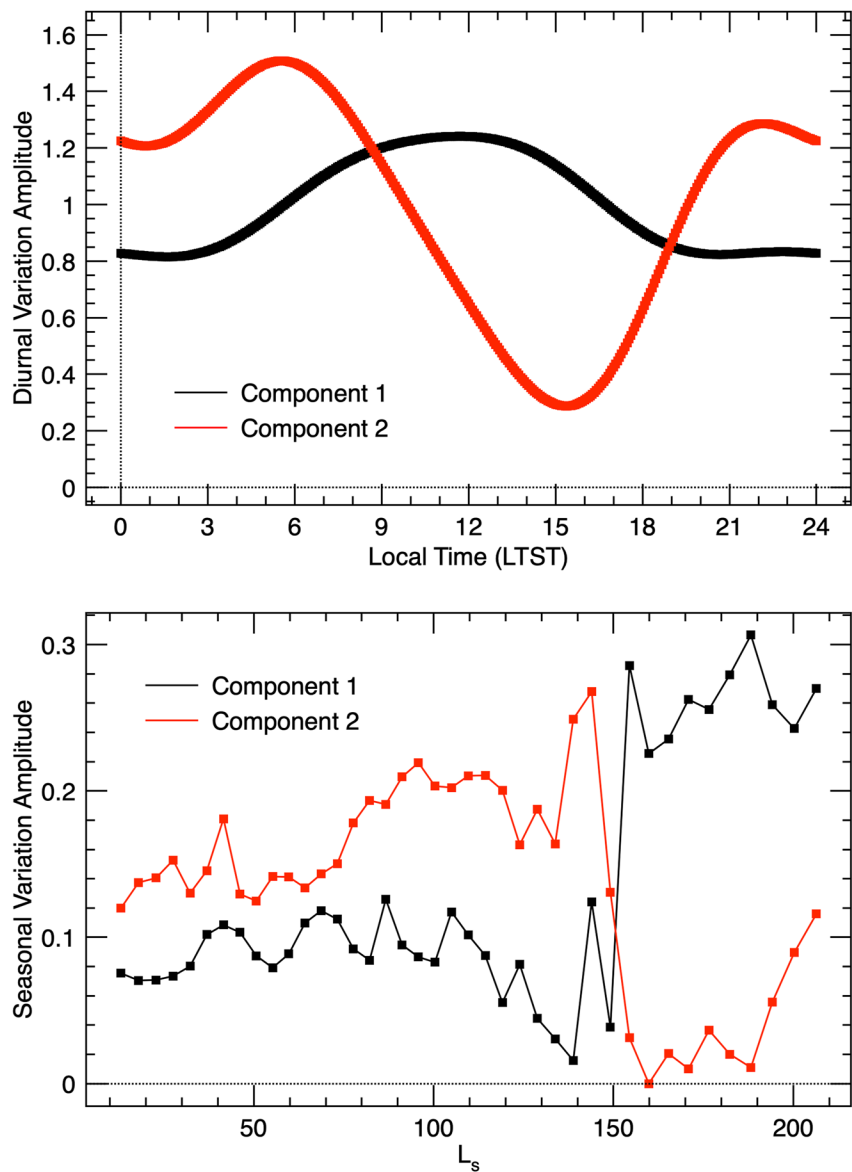


**Figure 7.** (Top panel) The diurnal variation (the  $D_1$  and  $D_2$  functions of Equations 1 and 2) of the two components that best fit the retrieved Thermal InfraRed Sensor (TIRS) aerosol optical depths. (Bottom panel) The variation with  $L_s$ , or sol (the  $S_1$  and  $S_2$  functions in Equation 1), of the two components that best fit the observed TIRS aerosol optical depths. Component 1 can be associated with dust aerosol, while component 2 can be associated with water ice cloud aerosol.

aerosols while component 2 represents water ice clouds. Note that the spike in dust from the dust storm itself is not represented here since those data were excluded from this analysis.

The identification of the two components cannot be considered definitive, especially since this solution is not unique. Indeed, any linear combination of the two diurnal variation functions  $D_1$  and  $D_2$ , along with correspondingly modified  $S_1$  and  $S_2$ , would result in exactly the same fit. However, the seasonal variations presented in the bottom panel of Figure 7 align well with the expected variations of dust and water ice cloud (M. D. Smith et al., 2022), and so this identification is useful. Figure 8 shows a comparison of the retrieved TIRS total aerosol optical depth and the best-fit optical depth obtained using Equation 1 with the 90 best-fit parameters. There are details that are missed by the fit (notably the dust storm which was not included in the fit), but overall, this parameterization describes both the diurnal and seasonal variations quite well.

Assuming the association of component 1 with dust and component 2 with water ice cloud, Figure 7 can be used to identify the average diurnal and seasonal trends of the two aerosols. In this interpretation, water ice clouds

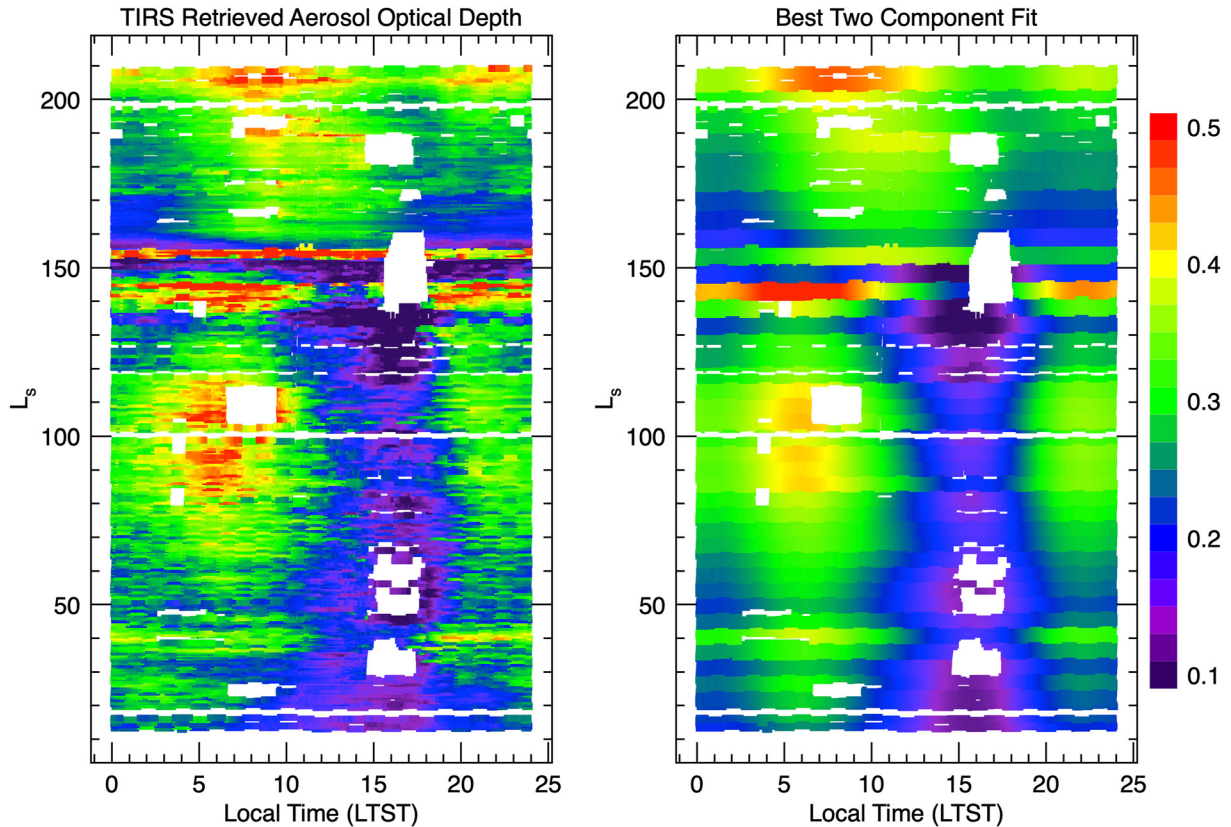


**Figure 8.** Comparison of (left panel) the total aerosol optical depth retrieved from Thermal InfraRed Sensor (TIRS) with (right panel) a reconstruction of the best-fit aerosol optical depth using the two-component fit. The two-component fit does not attempt to fit the regional dust storm at  $L_s = 153^\circ$ , but otherwise represents quite well the other main seasonal and diurnal variations observed by TIRS.

over the Perseverance rover during the aphelion season have their maximal diurnal opacity just before dawn, their diurnal minimum value in the late afternoon, and a secondary maximum in the evening a couple of hours past sunset. The peak-to-peak diurnal variation is large, roughly a factor of five. On the other hand, dust exhibits a more modest variation with a broad maximum during midday and 30% lower values throughout the night. As a function of season ( $L_s$ ), the optical depth of dust was roughly steady at a low baseline level before  $L_s = 150^\circ$  while the optical depth of water ice was greater than that of dust rising to a peak around  $L_s = 100^\circ$ . After the regional dust storm ( $L_s = 153^\circ$ ), dust remained elevated while the water ice clouds largely disappeared before beginning to come back somewhat after  $L_s = 190^\circ$ .

The diurnal variations for dust (component 1) and water ice cloud (component 2) described above can be compared against observations from other spacecraft. For water ice cloud, a minimum optical depth in the middle of the day with higher amounts near dawn and dusk has been noted previously in retrievals from, for example, the THEMIS instrument on Mars Odyssey (M. D. Smith, 2019), the PFS instrument on Mars Express (Giuranna et al., 2021), and the EMIRS instrument on the Emirates Mars Mission (Atwood et al., 2022). Giuranna et al. (2021) also found dust optical depths to be higher during the day than at night, consistent with the diurnal variation observed for TIRS component 1. The MCD model results (Forget et al., 1999; Millour et al., 2018) show little diurnal variation for dust, but for water ice cloud, the diurnal variation is very similar in character to that of TIRS, with a midday minimum, diurnal maximum near dawn, and a secondary maximum in the late evening before midnight.

#### 4.2. Comparison With MEDA SkyCam Aerosol Optical Depth

The SkyCam is a zenith-viewing wide-angle camera that is a part of the MEDA suite of instruments on Perseverance (J. A. Rodriguez-Manfredi et al., 2021). It is based on the HazCams from the Mars Exploration Rovers and Mars Science Laboratory (J. Maki et al., 2012; J. N. Maki et al., 2003), and contains a neutral density filter

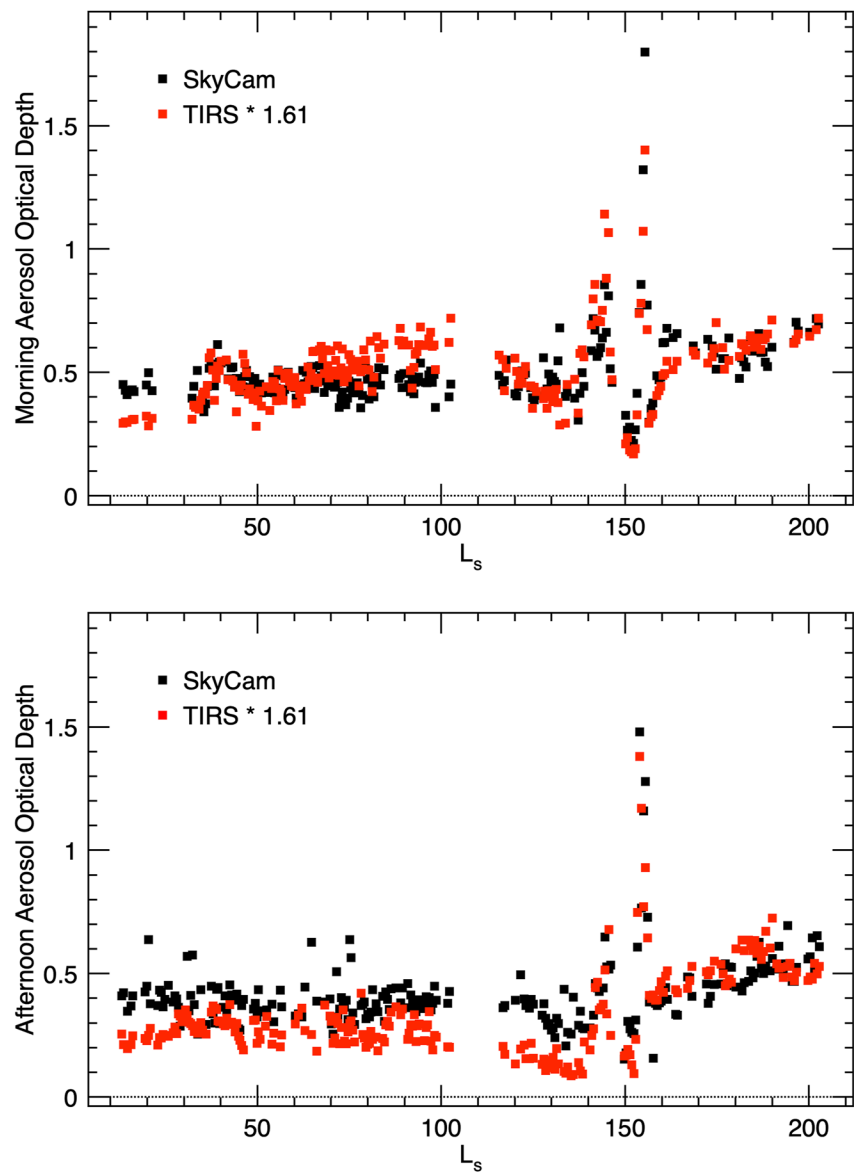


**Figure 9.** A comparison of the total aerosol optical depth retrieved from Thermal InfraRed Sensor (TIRS) (red points) compared to those from SkyCam (black points). The TIRS optical depths have all been multiplied by a constant factor of 1.61 to account for the wavelength difference between the two instruments. (Top panel) Comparison of morning SkyCam observations (typically 8:00–09:00 local true solar time [LTST]). (Bottom panel) Comparison of afternoon SkyCam observations (typically 14:00–15:30 LTST).

in the form of an annulus that enables the direct observation of total aerosol optical depth at an effective wavelength of 694 nm when the Sun passes behind the filter, nominally twice per sol during the mid-morning and mid-afternoon.

SkyCam images are routinely taken each sol as part of the normal observation sequences of MEDA, and so the TIRS and SkyCam retrievals of total aerosol optical depth can be directly compared. Figure 9 shows this comparison separately for the morning (~08:00–09:00) and afternoon (~14:00–15:30) SkyCam observations. The TIRS retrievals have been multiplied by a constant factor of 1.61 (determined as the single overall best-fit ratio between the SkyCam and TIRS optical depths) to account for the differences between the aerosol optical depth reported at visible wavelengths by SkyCam and at thermal infrared wavelengths by TIRS.

The agreement between the two instruments is quite good for the morning observations shown in the top panel of Figure 9. Both instruments observed the aphelion cloud belt, with the early and late season peaks at  $L_s = 40^\circ$

and  $140^\circ$ , as well as the regional dust storm at  $L_s = 153^\circ$  and the elevated (dust) aerosol opacity after that. However, the agreement was not nearly as good for the afternoon observations. In particular, during the period before  $L_s = 140^\circ$  dominated by water ice clouds, the TIRS retrieved total aerosol optical depth is systematically lower than that from SkyCam, even after multiplying by 1.61 to account for the nominal difference caused by the wavelength difference between the two instruments. It is notable that the afternoon observations do show good agreement once dust becomes the dominant aerosol after  $L_s = 150^\circ$ .

The difference in observed afternoon aerosol optical depth between TIRS and SkyCam appears to be caused primarily by something related to water ice clouds. In both the SkyCam and the TIRS retrievals, the morning aerosol optical depths are greater than those in the afternoon. However, while for SkyCam the difference is about 20%–30%, for TIRS the difference is roughly a factor of 2. To investigate this difference, it is useful to further explore some of the key assumptions used in the TIRS retrieval. The two most important assumptions that likely bear on this problem are the vertical distribution of the water ice cloud and the particle size distribution of the water ice aerosols.

The top panel of Figure 10 shows the result of a numerical experiment where the TIRS retrieval has been run for sols 149 and 150 ( $L_s = 75^\circ$ ) with the water ice clouds being placed at different heights, either right at the surface, at one scale height above the surface (the nominal case), or at two scale heights above the surface. As the cloud moves higher in the atmosphere, it is at cooler temperatures and thus more optical depth is required to produce the observed signal given by TIRS IR1. The bottom panel of Figure 10 shows the ratio between the optical depth at the wavelength of SkyCam (694 nm) and the optical depth at the wavelength of TIRS (12  $\mu\text{m}$ ) using Mie Theory. Because the TIRS optical depth (for water ice aerosol) is always referenced to  $825 \text{ cm}^{-1}$  (or 12  $\mu\text{m}$ ), it doesn't change with a change in the assumed particle size of the water ice aerosol, but its relation to the corresponding SkyCam optical depth does change.

Until this point we have made the assumption that the vertical distribution of the aerosols and the effective particle size of the aerosols are constant and do not change as a function of season or LT. However, the results of the numerical experiments shown in Figure 10 demonstrate that a cloud height or water ice particle size that changes from morning to afternoon could potentially explain the difference in the afternoon retrievals of optical depth between SkyCam and TIRS. In particular, a cloud height that increased from morning to afternoon and an effective water ice particle size that decreased from morning to afternoon would both be in the correct sense to bring the SkyCam and TIRS retrievals into agreement.

Numerous previous studies have demonstrated that the effective radii of dust and water ice aerosols do change with season (e.g., Clancy et al., 2003; Guzewich & Smith, 2019; Vicente-Retortillo et al., 2017; Wolff et al., 2006), and thus it seems possible (at least for water ice) that the effective radius of the particles could change diurnally as well. Likewise, given that the vertical location of clouds in the atmosphere is controlled by condensation dynamics and the temperature structure, it would not be surprising if the base of the cloud layer moved upward during the day as the planetary boundary layer expands and temperatures warm in the lowest portion of the atmosphere. Indeed, MCD model results (Forget et al., 1999; Millour et al., 2018) show the base of the cloud layer moving upward between dawn and mid-afternoon. Other possible explanations that could explain the afternoon difference between SkyCam and TIRS, including a systematic error in the diurnal variation of our assumed temperature profile (which would need to be  $\sim 10$ – $20$  K) and calibration errors in the TIRS data with a systematic diurnal pattern, would need to be present only during the aphelion season and seem less likely. We therefore consider the mismatch between SkyCam and TIRS aerosol optical depth to be evidence of diurnal variations in either cloud height or cloud particle size or both.

## 5. Conclusions and Summary

With more than an Earth year of observations from the MEDA instrument suite on-board the Perseverance rover, the two upward-looking TIRS sensors have provided a unique data set in its ability to provide systematic retrievals of total aerosol optical depth as a function of LT and season, including both during the day and the night. The retrieved values reveal clear seasonal and diurnal variations in aerosol optical depth.

During the aphelion season, we find the water ice clouds are the largest source of aerosol optical depth. For these water ice clouds, the two dominant patterns involve the seasonal growth and decay of the aphelion clouds and a consistent diurnal pattern. The cloud optical depth gradually increased from the beginning of Perseverance

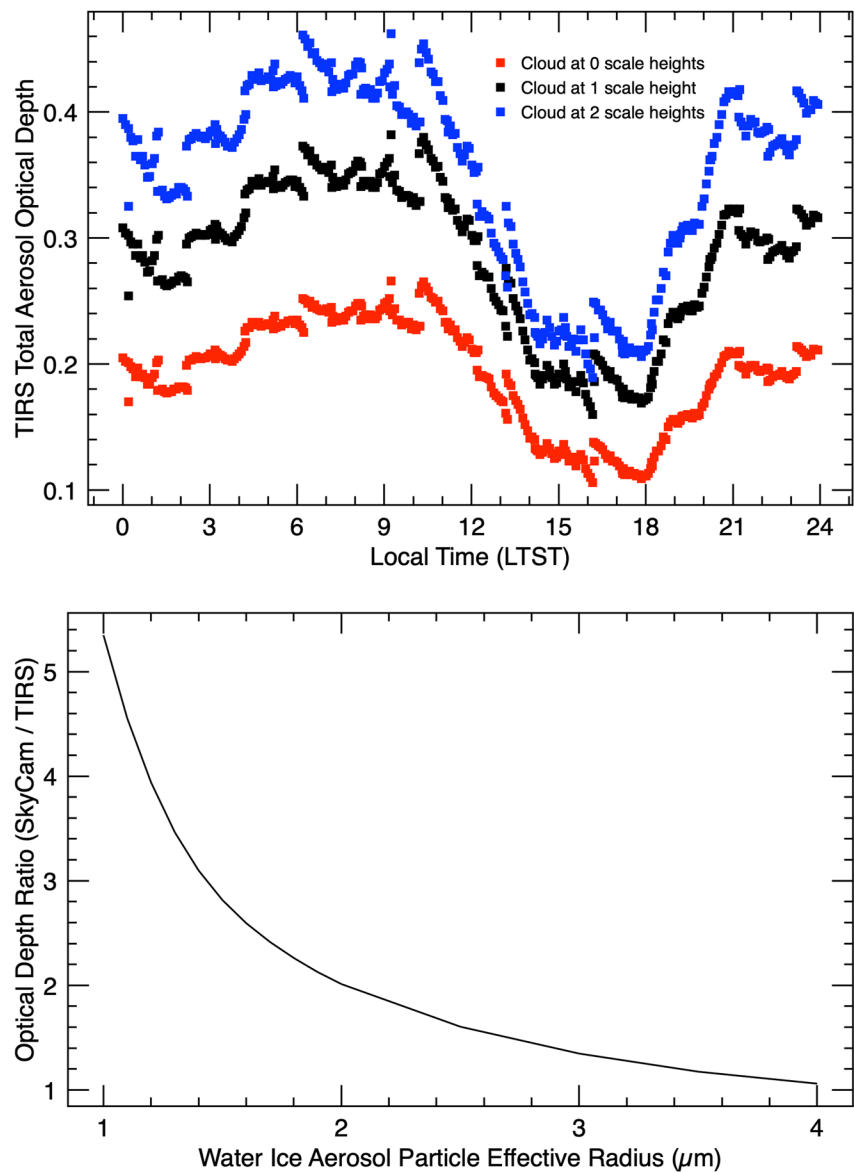


**Figure 10.** (Top panel) The retrieved total aerosol optical depth from Thermal InfraRed Sensor (TIRS) observations taken during sols 149 and 150 ( $L_s = 75^\circ$ ), typical of those taken during the aphelion season. Three different cases are shown with the base of the water ice cloud being placed at the surface (red), at one scale height above the surface (black, the nominal assumption), and at two scale heights above the surface (blue). (Bottom panel) The ratio of optical depth between SkyCam and TIRS wavelengths for water ice aerosols as a function of the effective radius of the particles.

observations ( $L_s = 13^\circ$ ) until reaching a maximum around  $L_s = 100^\circ$ , which was followed by a more rapid decrease. Brief increases in cloud optical depth were observed both early ( $L_s = 40^\circ$ ) and late ( $L_s = 140^\circ$ ) in the season. The diurnal variation of clouds consistently showed a diurnal maximum at 06:00, a diurnal minimum at 16:00, and a secondary maximum at 22:00. The maximum cloud optical depth was approximately 0.3 (referenced to  $825 \text{ cm}^{-1}$  or  $12 \mu\text{m}$ ) at 06:00 LT at  $L_s = 100^\circ$ . Significant sol-to-sol variations were observed in cloud opacity with the greatest variations occurring at night, highlighting the value of the TIRS retrievals, which can be performed for all local times.

A large regional dust storm was observed by Perseverance during early January 2022 ( $L_s = 153^\circ$ ). The most active period of this storm lasted 6 sols, and the TIRS retrievals show numerous spikes of dust lasting hours and reach optical depths of 0.7 or greater. This demonstrates the utility of the ability of TIRS to retrieve optical depth values continuously whenever MEDA takes observations for better understanding the complex evolution of aerosol

optical depth during the active portion of a dust storm. After the regional dust storm, the TIRS retrievals showed that dust dominated the total aerosol optical depth, and that the diurnal variation was different with maximal diurnal values closer to noon.

Comparison of the TIRS retrievals of aerosol optical depth with simultaneous observations by the SkyCam instrument, which is also part of the MEDA instrument suite, shows a discrepancy between morning and afternoon observations that is indicative of possible diurnal variations in either the height of water ice clouds or the effective radius of the water ice particles, or both.

Systematic TIRS observations continue as part of the baseline set of MEDA observations on the Perseverance rover. These observations will extend the existing record through the remainder of the perihelion season, promising exciting new information about the diurnal and seasonal variation of aerosols throughout an entire Martian year.

### Data Availability Statement

All data used in this study from the Perseverance rover are available from the Planetary Data System (PDS). In particular, the MEDA data are available at: J. Rodriguez-Manfredi and de la Torre Juarez (2021). The retrieval results for total aerosol optical depth from TIRS are available in an archive located at: M. D. Smith (2022).

### References

- Atwood, S. A., Smith, M. D., Badri, K., Edwards, C. S., Christensen, P. R., Wolff, M. J., et al. (2022). Diurnal variability in EMIRS daytime observations of water ice clouds during Mars aphelion season. *Geophysical Research Letters*, *49*(15), e2022GL099654. <https://doi.org/10.1029/2022GL099654>
- Chen-Chen, H., Pérez-Hoyos, S., & Sánchez-Lavega, A. (2019). Dust particle size and optical depth on Mars retrieved by the MSL navigation cameras. *Icarus*, *319*, 43–57. <https://doi.org/10.1016/j.icarus.2018.09.010>
- Christensen, P. R., Mehall, G. L., Silverman, S. H., Anwar, S., Cannon, G., Gorelick, N., et al. (2003). Miniature thermal emission spectrometer for the Mars exploration rovers. *Journal of Geophysical Research*, *108*(312), 8064. <https://doi.org/10.1029/2003JE002117>
- Clancy, R. T., Montmessin, F., Benson, J., Daerden, F., Colaprete, A., & Wolff, M. J. (2017). Mars clouds. In *Chapter 5 in "The atmosphere and climate of Mars"*. Cambridge University Press. <https://doi.org/10.1017/9781139060172.005>
- Clancy, R. T., Wolff, M. J., & Christensen, P. R. (2003). Mars aerosol studies with the MGS TES emission phase function observations: Optical depths, particle sizes, and ice cloud types versus latitude and solar longitude. *Journal of Geophysical Research*, *108*(E9), 5098. <https://doi.org/10.1029/2003JE002058>
- Colburn, D. S., Pollack, J. B., & Haberle, R. M. (1989). Diurnal variations in optical depth at Mars. *Icarus*, *79*(1), 159–189. [https://doi.org/10.1016/0019-1035\(89\)90114-0](https://doi.org/10.1016/0019-1035(89)90114-0)
- Conrath, B. J. (1975). Thermal structure of the Martian atmosphere during the dissipation of the dust storm of 1971. *Icarus*, *24*(1), 36–46. [https://doi.org/10.1016/0019-1035\(75\)90156-6](https://doi.org/10.1016/0019-1035(75)90156-6)
- Edwards, C. S., Christensen, P. R., Mehall, G. L., Anwar, S., Tunajji, E. A., Badri, K., et al. (2021). The Emirates Mars Mission (EMM) Emirates Mars InfraRed Spectrometer (EMIRS) instrument. *Space Science Reviews*, *217*(7), 77. <https://doi.org/10.1007/s11214-021-00848-1>
- Forget, F., Hourdin, F., Fournier, R., Hourdin, C., Talagrand, O., Collins, M., et al. (1999). Improved general circulation models of the Martian atmosphere from the surface to above 80 km. *Journal of Geophysical Research*, *104*(E10), 24155–24175. <https://doi.org/10.1029/1999je001025>
- Gierasch, P. J., & Goody, R. M. (1972). The effect of dust on the temperature of the Martian atmosphere. *Journal of the Atmospheric Sciences*, *29*(2), 400–402. [https://doi.org/10.1175/1520-0469\(1972\)029<0400:teodot>2.0.co;2](https://doi.org/10.1175/1520-0469(1972)029<0400:teodot>2.0.co;2)
- Giuranna, M., Wolkenberg, P., Grassi, D., Aronica, A., Aoki, S., Scaccabarozzi, D., et al. (2021). The current weather and climate of Mars: 12 years of atmospheric monitoring by the planetary Fourier spectrometer on Mars express. *Icarus*, *353*, 113406. <https://doi.org/10.1016/j.icarus.2019.113406>
- Guzewich, S. D., & Smith, M. D. (2019). Seasonal variation in Martian water ice cloud particle size. *Journal of Geophysical Research: Planets*, *124*(2), 636–643. <https://doi.org/10.1029/2018JE005843>
- Kahre, M. A., Murphy, J. R., & Haberle, R. M. (2006). Modeling the Martian dust cycle and surface dust reservoirs with the NASA Ames general circulation model. *Journal of Geophysical Research*, *111*(E6), E06008. <https://doi.org/10.1029/2005JE002588>
- Kahre, M. A., Murphy, J. R., Newman, C. E., Wilson, R. J., Cantor, B. A., Lemmon, M. T., & Wolff, M. J. (2017). The Mars dust cycle. In *Chapter 10 in "The atmosphere and climate of Mars"*. Cambridge University Press. <https://doi.org/10.1017/9781139060172.010>
- Lacis, A. A., & Oinas, V. (1991). A description of the correlated k distribution method for modeling nongray gaseous absorption, thermal emission, and multiple scattering in vertically inhomogeneous atmospheres. *Journal of Geophysical Research*, *96*(D5), 9027–9063. <https://doi.org/10.1029/90jd01945>
- Lemmon, M. T., Smith, M. D., Viudez-Moreiras, D., de la Torre, M., Vicente-Retortillo, A., Munguira, A., et al. (2022). Dust, sand, and winds within an active Martian storm in Jezero Crater. *Geophysical Research Letters*, *49*(17), e2022GL100126. <https://doi.org/10.1029/2022GL100126>
- Lemmon, M. T., Wolff, M. J., Bell, J. F., III, Smith, M. D., Cantor, B. A., & Smith, P. H. (2015). Dust aerosol, clouds, and the atmospheric optical depth record over 5 Mars years of the Mars Exploration Rover mission. *Icarus*, *251*, 96–111. <https://doi.org/10.1016/j.icarus.2014.03.029>
- Lemmon, M. T., Wolff, M. J., Smith, M. D., Clancy, R. T., Banfield, D., Landis, G. A., et al. (2004). Atmospheric imaging results from the Mars exploration rovers: Spirit and opportunity. *Science*, *306*(5702), 1753–1756. <https://doi.org/10.1126/science.1104474>
- Maki, J., Thiessen, D., Pourangi, A., Kobzeff, P., Litwin, T., Scherr, L., et al. (2012). The Mars science laboratory engineering cameras. *Space Science Reviews*, *170*(1–4), 77–93. <https://doi.org/10.1007/s11214-012-9882-4>
- Maki, J. N., Bell, J. F., III, Herkenhoff, K. E., Squyres, S. W., Kiely, A., Klimesh, M., et al. (2003). Mars Exploration rover engineering camera. *Journal of Geophysical Research*, *108*(E12), 8071. <https://doi.org/10.1029/2003JE002077>

### Acknowledgments

We would like to thank everyone who made the Perseverance mission possible. We especially thank the MEDA team for their efforts in obtaining this remarkable data set. G. Martínez would like to acknowledge JPL funding from USRA Contract 1638782. E. Sebastián would like to acknowledge funding from the Spanish Plan Estatal de I+D+I (ESP2014-54256-C4-1-R, ESP2015-68281-C4-1-R, ESP2016-79612-C3-1-R, RTI2018-099825-B-C31, and MDM-2017-0737). Portions of this research were carried out at the Jet Propulsion Laboratory, California Institute of Technology, under a contract with the National Aeronautics and Space Administration (80NM0018D0004). The NASA and JPL co-authors acknowledge funding from NASA's Game Changing Development and Space Technology Mission Directorate, NASA's Science Mission Directorate, and the Advanced Exploration Systems Program that resided in the previous Human Exploration and Operations Mission Directorate.

- Martínez, G. M., Sebastián, E., Vicente-Retortillo, A., Smith, M. D., Johnson, J. R., Fischer, E., et al. (2023). Surface energy budget, albedo and thermal inertia at Jezero Crater, Mars, as observed from the Mars 2020 MEDA instrument. *Journal of Geophysical Research*. <https://doi.org/10.1029/2022JE007537>
- Mason, E. L., & Smith, M. D. (2021). Temperature fluctuations and boundary layer turbulence as seen by Mars exploration rovers miniature thermal emission spectrometer. *Icarus*, *360*, 114350. <https://doi.org/10.1016/j.icarus.2021.114350>
- Millour, E., Forget, F., Spiga, A., Vals, M., Zakharov, V., & Montabone, L. (2018). The Mars climate database (version 5.3). In *Scientific workshop "From Mars express to ExoMars"*. ESAC.
- Newman, C. E., de la Torre, M., Pla-García, J., Wilson, R. J., Lewis, S. R., Neary, L., et al. (2021). Multi-model meteorological and aeolian predictions for Mars 2020 and the Jezero Crater Region. *Space Science Reviews*, *217*(1), 20. <https://doi.org/10.1007/s11214-020-00788-2>
- Newman, C. E., Lewis, S. R., Read, P. L., & Forget, F. (2002). Modeling the Martian dust cycle 2. Multiannual radiatively active dust transport simulations. *Journal of Geophysical Research*, *107*(E12), 5124–7–15. <https://doi.org/10.1029/2002JE001920>
- Pérez-Izquierdo, J., Sebastián, E., Martínez, G. M., Bravo, A., Ramos, M., & Rodríguez-Manfredi, J. A. (2018). The Thermal Infrared Sensor (TIRS) of the Mars Environmental Dynamics Analyzer (MEDA) instrument onboard Mars 2020, a general description and performance analysis. *Measurement*, *122*, 432–442. <https://doi.org/10.1016/j.measurement.2017.12.004>
- Petty, G. W. (2006). *A first course in atmospheric radiation* (2nd ed., p. 452pp). Sundog Publishing.
- Pla-García, J., Rafkin, S. C. R., Martínez, G. H., Vicente-Retortillo, A., Newman, C. E., Savijärvi, H., et al. (2020). Meteorological predictions for Mars 2020 perseverance rover landing site at Jezero Crater. *Space Science Reviews*, *216*(8), 148. <https://doi.org/10.1007/s11214-020-00763-x>
- Rafkin, S. C. R., Pla-García, J., Kahre, M., Gomez-Elvira, J., Hamilton, V. E., Marín, M., et al. (2016). The meteorology of Gale Crater as determined from Rover Environmental Monitoring Station observations and numerical modeling. Part II: Interpretation. *Icarus*, *280*, 114–138. <https://doi.org/10.1016/j.icarus.2016.01.031>
- Rodríguez-Manfredi, J., & de la Torre Juárez, M. (2021). Mars 2020 perseverance rover Mars environmental dynamics analyzer (MEDA) experiment data record (EDR) and reduced data record (RDR) data products archive bundle [Dataset]. PDS Atmospheres Node. <https://doi.org/10.17189/1522849>
- Rodríguez-Manfredi, J. A., de la Torre Juárez, M., Alonso, A., Apéstigue, V., Arruago, I., Atienza, T., et al. (2021). The Mars Environmental Dynamics Analyzer, MEDA. A suite of environmental sensors for the Mars 2020 mission. *Space Science Reviews*, *217*, 48. <https://doi.org/10.1007/s11214-021-00816-9>
- Sebastián, E., Martínez, G., Ramos, M., Haenschke, F., Ferrándiz, R., Fernández, M., & Rodríguez-Manfredi, J. A. (2020). Radiometric and angular calibration tests for the MEDA-TIRS radiometer onboard NASA's Mars 2020 mission. *Measurement*, *164*, 107968. <https://doi.org/10.1016/j.measurement.2020.107968>
- Sebastián, E., Martínez, G., Ramos, M., Pérez-Grande, I., Sobrado, J., & Rodríguez-Manfredi, J. A. (2021). Thermal calibration of the MEDA-TIRS radiometer onboard NASA's Perseverance rover. *Acta Astronautica*, *182*, 144–159. <https://doi.org/10.1016/j.actaastro.2021.02.006>
- Smith, M. D. (2004). Interannual variability in TES atmospheric observations of Mars during 1999–2003. *Icarus*, *167*(1), 148–165. <https://doi.org/10.1016/j.icarus.2003.09.010>
- Smith, M. D. (2019). Local time variation of water ice clouds on Mars as observed by THEMIS. *Icarus*, *333*, 273–282. <https://doi.org/10.1016/j.icarus.2019.06.009>
- Smith, M. D. (2022). Perseverance MEDA/TIRS aerosol retrievals [Dataset]. Mendeley Data Archive, V1. <https://doi.org/10.17632/48phhtkcj8.1>
- Smith, M. D., Badri, K., Atwood, S. A., Edwards, C. S., Christensen, P. R., Wolff, M. J., et al. (2022). EMIRS observations of the aphelion-season Mars atmosphere. *Geophysical Research Letters*, *49*(15), e2022GL099636. <https://doi.org/10.1029/2022GL099636>
- Smith, M. D., Wolff, M. J., Lemmon, M. T., Spanovich, N., Banfield, D., Budney, C. J., et al. (2004). First atmospheric science results from the Mars exploration rovers mini-TES. *Science*, *306*(5702), 1750–1753. <https://doi.org/10.1126/science.1104257>
- Smith, M. D., Wolff, M. J., Spanovich, N., Ghosh, A., Banfield, D., Christensen, P. R., et al. (2006). One Martian year of atmospheric observations using MER Mini-TES. *Journal of Geophysical Research*, *111*(E12), E12S13. <https://doi.org/10.1029/2006JE002770>
- Smith, M. D., Zorzano, M.-P., Lemmon, M., Martín-Torres, J., & Mendaza de Cal, T. (2016). Aerosol optical depth as observed by the Mars Science Laboratory REMS UV photodiodes. *Icarus*, *280*, 234–248. <https://doi.org/10.1016/j.icarus.2016.07.012>
- Smith, P. H., & Lemmon, M. (1999). Opacity of the Martian atmosphere measured by the Imager for Mars Pathfinder. *Journal of Geophysical Research*, *104*(E4), 8975–8985. <https://doi.org/10.1029/1998JE900017>
- Vicente-Retortillo, A., Martínez, G. M., Renno, N. O., Lemmon, M. T., & de la Torre, M. (2017). Determination of dust aerosol particle size at Gale Crater using REMS UVS and Mastcam measurements. *Geophysical Research Letters*, *44*(8), 3502–3508. <https://doi.org/10.1002/2017GL072589>
- Wolff, M. J., López-Valverde, M., Madeleine, J.-B., Wilson, R. J., Smith, M. D., Fouchet, T., & Delory, G. T. (2017). Radiative process: Techniques and applications. In *Chapter 6 in "The atmosphere and climate of Mars"*. Cambridge University Press. <https://doi.org/10.1017/9781139060172.006>
- Wolff, M. J., Smith, M. D., Clancy, R. T., Spanovich, N., Whitney, B. A., Lemmon, M. T., et al. (2006). Constraints on dust aerosols from the Mars Exploration Rovers using MGS overflights and Mini-TES. *Journal of Geophysical Research*, *111*(E12), E12S17. <https://doi.org/10.1029/2006JE002786>
- Wu, Z., Richardson, M. I., Zhang, X., Cui, J., Heavens, N. G., Lee, C., et al. (2021). Large eddy simulations of the dusty Martian convective boundary layer with MarsWRF. *Journal of Geophysical Research: Planets*, *126*(9), e2020JE006752. <https://doi.org/10.1029/2020JE006752>